ACS OMEGA

http://pubs.acs.org/journal/acsodf

Article

Enhancing Structural Properties and Performance of Graphene-Based Devices Using Self-Assembled HMDS Monolayers

Sami Ramadan,* Yuanzhou Zhang, Deana Kwong Hong Tsang, Olena Shaforost, Lizhou Xu, Ryan Bower, Iain E. Dunlop, Peter K. Petrov, and Norbert Klein

Cite This: *ACS Omega* 2021, 6, 4767−4775

Read Online

ACCESS | Metrics & More | Article Recommendations | Supporting Information

ABSTRACT: The performance of graphene devices is often limited by defects and impurities induced during device fabrication. Polymer residue left on the surface of graphene after photoresist processing can increase electron scattering and hinder electron transport. Furthermore, exposing graphene to plasma-based processing such as sputtering of metallization layers can increase the defect density in graphene and alter the device performance. Therefore, the preservation of the high-quality surface of graphene during thin-film deposition and device manufacturing is essential for many electronic applications. Here, we show that the use of self-assembled monolayers (SAMs) of hexamethyldisilazane (HMDS) as a buffer layer during the device fabrication of graphene can significantly reduce damage, improve the quality of graphene, and enhance device performance. The role of HMDS has been systematically investigated using surface analysis techniques and electrical measurements. The benefits of HMDS treatment include a significant reduction in defect density compared with as-treated graphene and more than a 2-fold reduction of contact resistance. This surface treatment is simple and offers a practical route for improving graphene device interfaces, which is important for the integration of graphene into functional devices such as electronics and sensor devices.

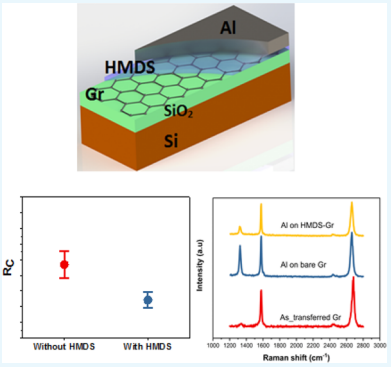

1. INTRODUCTION

Graphene has demonstrated excellent electrical, mechanical, and optical properties that make it ideal as a building block for numerous device applications.[1,2] Near ballistic transport and high carrier mobility make it a suitable candidate for the next generation of nanoelectronics, especially high-frequency devices.[3,4] Furthermore, graphene has been proposed in many other device applications such as terahertz,[5−7] nano-electromechanical systems,[8,9] solar cells,[10] gas sensors,[11−13] and biosensors.[14−16] However, the device performance is often limited by structural defects and damage introduced during different stages of fabrication and processing. This results in increased device scattering and contact resistance, affecting device performance. Modern device fabrication involves photolithography, etching, and thin-film deposition. However, implementing these steps on two-dimensional (2D) materials has been associated with many issues, such as the tearing of graphene, introduction of unintentional doping, increased damage to devices, and higher defect density in graphene.[17] For instance, the use of plasma and ion bombardment during sputtering has been frequently reported to increase damage to graphene,[18−20] degrade device properties, and increase contact resistance.[21] Moreover, polymer residues left on the surface of graphene after photolithography are difficult to be removed completely and can degrade device performance.[22,23] Several approaches have been implemented to reduce the defect density and degradation of devices during lithography or sputtering for the improvement of device performance. Some approaches include annealing[24] or the insertion of sacrificial layers of AlOx[25,26] and Au,[27] aiming to passivate the device during the fabrication process.

Self-assembled monolayers (SAMs) have been widely used to tune the electronic properties of 2D materials and to improve device performance.[28,29] For instance, inserting hydrophobic SAMs as a buffer layer between the graphene and SiO_2/Si substrate has been reported to control the electrical properties of graphene-field-effect transistors (GFETs) and to reduce hysteresis behavior in GFET characteristics.[30,31] Furthermore, the application of perfluorodecyltrichlorosilane (FDTS)[32] or hexamethyldisilazane (HMDS)[33] prior to chemical vapor deposition (CVD) and atomic layer deposition (ALD) processes has been demonstrated to enhance the coating of different dielectric films on graphene. Finally, it has been demonstrated that the mechanical properties of graphene can be modified by the hydrophobicity of the surface introduced by SAMs.[34]

Received: November 18, 2020
Accepted: January 27, 2021
Published: February 9, 2021

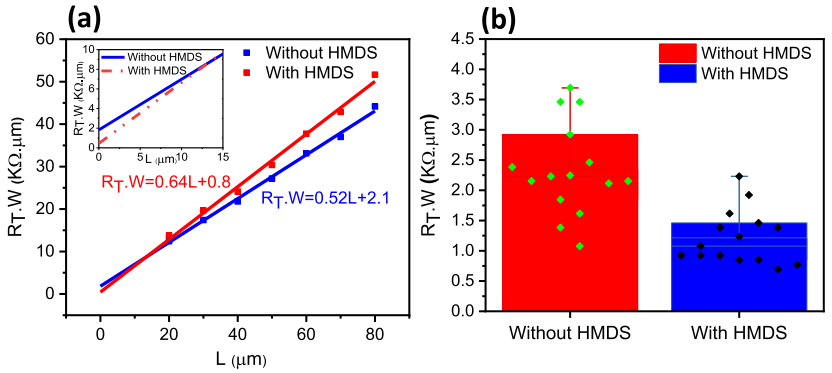

Figure 1. (a) Total contact resistance for CTLM devices with and without HMDS treatment (the inset is a magnification of the interception with *y*-axis). (b) Contact resistance for devices with and without HMDS treatment (error bars represent the data range within 1.5* interquartile range).

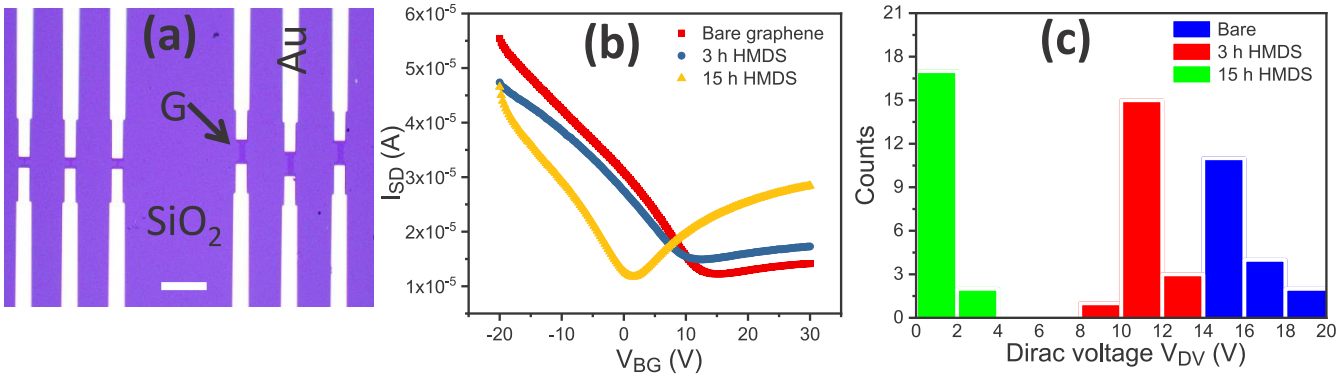

Figure 2. (a) Optical image of the GFET structure being used. (b) Transfer characteristics of GFETs with different treatment times of graphene with HMDS. (c) Histogram shows the Dirac point of GFETs with and without HMDS treatment. The scale bar in (a) is 50 μm.

Although some work has been performed to improve the GFETs using HMDS,[35,36] its role on the surface of graphene has not yet been fully investigated. This paper describes a systematic study of graphene modified with HMDS using surface analysis techniques, showing how its electronic properties are altered after HMDS treatment. We also show how treatment conditions can affect the properties of graphene.

This paper demonstrates the importance of incorporating self-assembled monolayers of HMDS at the graphene interface during device manufacturing and their role in improving the structural properties of graphene and device performance. We show how this can affect each step during device fabrication and the property of a device. By applying HMDS to graphene prior to the sputtering process, we observed a significant reduction in defect density of graphene after film deposition and a reduction of contact resistance. We also found an improvement in the surface quality of graphene when HMDS was applied prior to photoresist coating. This approach is simple and can be incorporated during the manufacturing process to reduce damage to graphene and to enhance the performance of graphene-based devices.

2. RESULTS AND DISCUSSION

2.1. Effect of HMDS on Contact Resistance and GFET Device Performance. The circular transmission line method (CTLM) is used to extract contact characteristics and values of the sheet resistance of graphene.[37,38] The method is chosen because of its simplicity and the fact that it does not require the fabrication of mesa structures. Therefore, there is no need for any further lithography step, thus avoiding problems of doping and the effect of polymer residues on the surface associated with photolithography. Measurements have been obtained for more than 12 devices for each type of treatment. Figure S1 shows a representative plot of $I-V$ at different spacings for both as-transferred and HMDS-treated samples. The HMDS treatment was performed for 15 h in the exposed graphene region after patterning and before the deposition of the contacts. The total resistance $R_T(W)$ as a function of spacing distance L is plotted in Figure 1a for devices with and without HMDS. The contact resistance is obtained from the *y*-axis intercept of the CTLM. A more than 2-fold reduction in contact resistance is observed after HMDS treatment, as can be seen from the histogram in Figure 1b.

This improvement in contact resistance after HMDS treatment gives an indication that HMDS acts as a protective layer and reduces the damage caused during sputtering and the contamination introduced during device processing. Another possible reason for the improvement in specific contact resistivity is an increase in work function difference between graphene and metal contacts with HMDS treatment compared with as-transferred graphene. This may lead to an increase of the charge transfer from the graphene to metals due to an increased density of the states of graphene underneath the contact area.[39]

Further improvement in contact resistance is achieved after postprocessing annealing at 210 °C in Ar ambient for 3 h. The contact resistance of HMDS-treated samples was reduced from (1200 ± 90) to (810 ± 79) Ω·μm. This value is much lower

https://dx.doi.org/10.1021/acsomega.0c05631
ACS Omega 2021, 6, 4767−4775

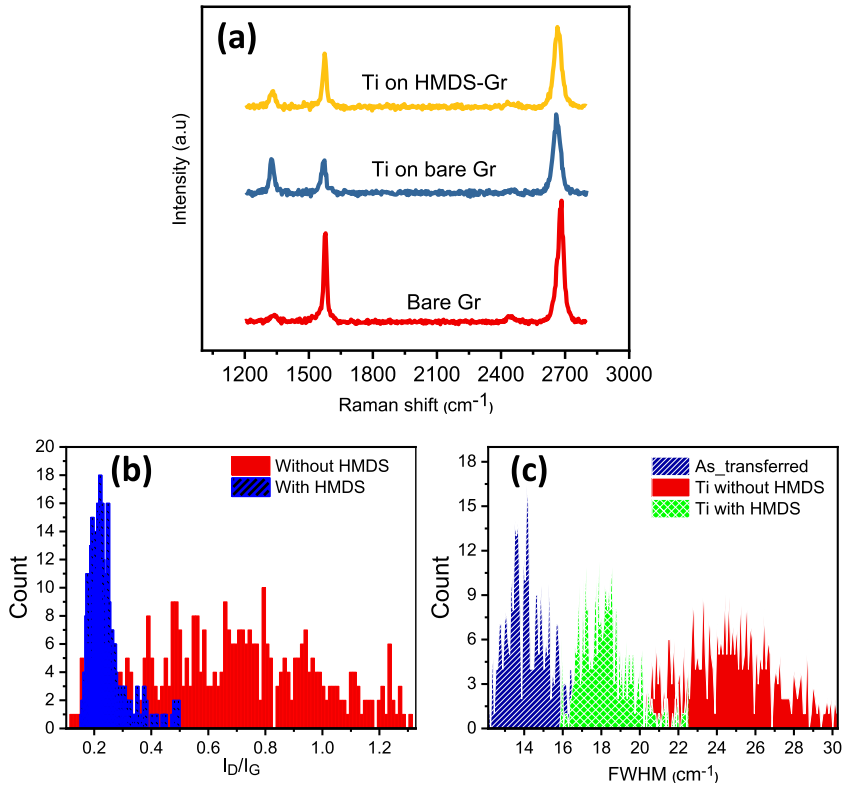

Figure 3. (a) Raman spectra of graphene with and without HMDS after DC sputtering deposition of Ti compared with as-transferred graphene. (b) I_D/I_G of graphene after Ti deposition for unprotected and protected samples with HMDS. (c) FWHM of (G) peak of graphene with and without HMDS after DC sputtering deposition of Ti compared with as-transferred graphene.

than the reported values of contact resistance for metal contacts deposited on graphene by sputttering.[40−43]

An improvement in GFETs characteristic after HMDS treatment has been reported recently.[35,36] HMDS can remove oxygen and water molecules absorbed on graphene surface and some polymer residues that act as charged impurity scattering center and degrading device performance.[35,36] Here, we repeatedly observed a Dirac point near zero after HMDS treatment (Figure 2b,c), compared with around 15 V for bare graphene. This shift in Dirac voltage can be used to calculate the shift in Fermi energy in graphene induced after HMDS. The Fermi energy shift is calculated according to the approximation assuming a linear band structure

$$\Delta E = \hbar v_F \sqrt{\pi n_i} \tag{1}$$

where v_F is the Fermi velocity in monolayer graphene of 1.1×10^6 m/s, n_i is the intrinsic carrier concentration, which can be written as $n_i = \eta(V_{DHMDS} - V_{DBARE})$[44] where $\eta \approx 7.210^{10}$ cm^{-2}. V^{-1} is the intrinsic carrier concentration per volt,[44,45] and V_{DHMDS} and V_{DBARE} are the Dirac voltages with and without HMDS treatment, respectively. The observed shift in Fermi level after HMDS is around 0.14 eV. More than 30% increase in hole mobility and around 100% increase in electron mobility were observed after HMDS treatment (Figure S2). The mobility is calculated from the transfer curve in the linear regime using the following equation

$$\mu = \frac{L}{W}\frac{g_m}{C_{ox}V_{SD}} \tag{2}$$

where $g_m = \frac{\Delta I_D}{\Delta V_G}$ in the linear region of the measure IV characteristic, C_{ox} oxide capacitance, V_{SD} is the source−drain voltage, and L and W are the length and the width of graphene structure, respectively.

2.2. Effect of Sputtering on As-Transferred and HMDS-Treated Graphene. Figure 3a shows a representative Raman spectrum of as-transferred graphene after 3 nm titanium sputtered on bare graphene and on HMDS-treated graphene. The D-peak located at 1346 cm^{-1} is observed after titanium deposition and film deposition. The D-peak indicates a structural disorder induced in sp^2 graphene due to defects. However, a significant reduction in D-peak intensity is visible for the sample treated with HMDS. The I_D/I_G extracted from the Raman map is plotted for both cases in Figure 3b. The values for position (G), full width at half-maximum (FWHM)-(G), and I_D/I_G for the as-transferred sample after Ti deposition are 1589 cm^{-1}, 24.4 ± 2.5 cm^{-1}, and 0.75, respectively. The value of I_D/I_G is reduced after HMDS treatment to 0.2 and FWHM(G) is 18.1 ± 2.2 cm^{-1}, while its position (G) is 1587 cm^{-1}. The increase in I_D/I_G and FWHM(G) for untreated samples is a sign of an increase in disorder of graphene for the as-transferred sputtered sample compared with the HMDS-treated one. The histogram of FWHM(G) is shown in Figure 3c. We also determined if there is any stain or doping induced in the film after metal deposition by calculating the ratio

$$\frac{\Delta\omega_{2D}}{\Delta\omega_G} = \frac{\omega_{2D} - \omega_{2D}^0}{\omega_G - \omega_G^0} \tag{3}$$

The values of Raman frequencies of 2D (ω_{2D}) and G (ω_G) modes are sensitive to charge impurities and strain in graphene.[46] We found that the average value of $\frac{\Delta\omega_{2D}}{\Delta\omega_G}$ for as-transferred devices is 0.78 ± 0.2, which corresponds to hole

https://dx.doi.org/10.1021/acsomega.0c05631
ACS Omega 2021, 6, 4767−4775

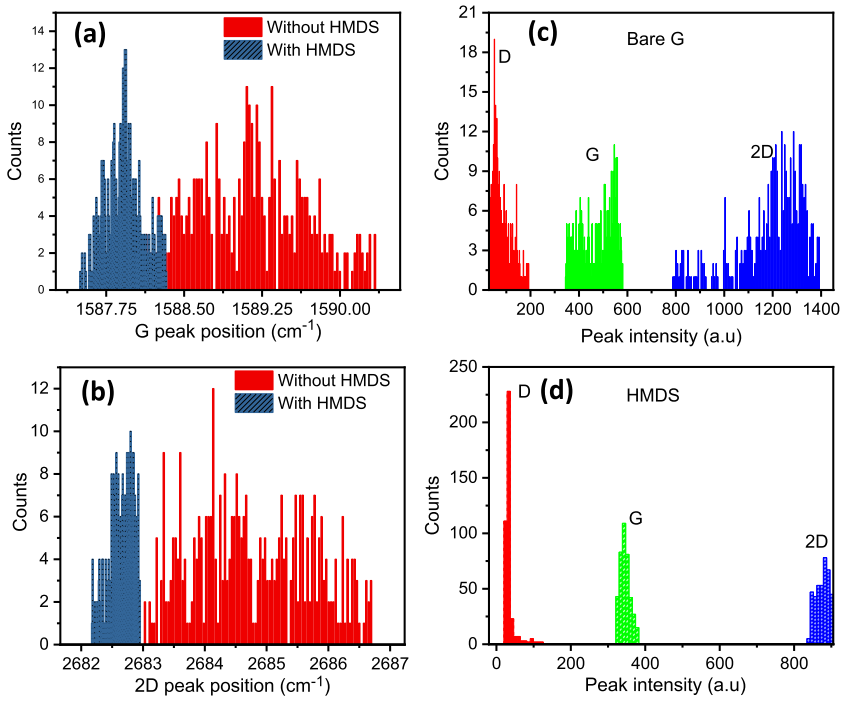

Figure 4. (a) G peak position of as-transferred and HMDS-treated graphene after photoresist removal. (b) Two-dimensional position of as-transferred and HMDS-treated graphene after photoresist removal. (c) Distribution of D, G, and 2D peak intensities of the as-transferred graphene sample after photoresist. (d) Distribution of D, G, and 2D peak intensities of the HMDS-treated graphene sample after photoresist.

doping, while the average values of $\frac{\Delta\omega_{2D}}{\Delta\omega_G}$ after Ti deposition for as-transferred and HMDS-treated samples are 0.85 ± 0.3 and 0.47 ± 0.2, respectively. Here, the intrinsic frequencies (ω_G^0 and ω_{2D}^0) are considered the values of freestanding graphene 1581.6 and 2676.9 cm^{-1}, respectively.[46] Since the value of $\frac{\Delta\omega_{2D}}{\Delta\omega_G} \ll 2$, this indicates that no strain has been induced after Ti deposition. However, these values show that graphene in the HMDS-treated samples is n-doped, while in the as-transferred samples it is p-doped.

We further calculated the defect concentration induced during the sputtering process for both cases. Considering samples with low degree of disorder (L_D > 10 nm), the defect concentration is given by[47,48]

$$n_D(cm^{-2}) = \frac{10^{14}}{L_D^2} \approx 1.8 \times 10^{10}(E_L)^4\left(\frac{I_D}{I_G}\right)_0 \quad (4)$$

where E_L is the excitation energy of the Raman laser (E_L = 2.33 eV) and L_D is the distance between two defects in nm. The defect density in graphene induced by sputtering is determined to be $n_{D\_HMDS} = 1.1 \times 10^{11}$ cm^{-2} for the HMDS-treated sample and $n_{D\_as\_tr} = 3.9 \times 10^{11}$ cm^{-2} for the as-transferred sample without treatment. These values correspond to L_{D_HMDS} = 30 nm and $L_{D\_as\_tr}$ = 16 nm. The values of n_D and L_D observed after HMDS treatment are typical values reported in CVD pristine graphene.[49,50] The reduction of disorder in graphene after HMDS treatment indicates that HMDS acts as a protective layer for graphene that reduces damage during the fabrication process. Reductions of damage are observed for both rf and dc sputtering and different films, as shown in Figure S3 (see the Supporting Information). This approach can be incorporated during sputtering thin-film deposition of metals and dielectric materials to graphene FETs while preserving the high quality of underlying graphene. The HMDS can be easily removed from the graphene interface by a simple annealing process of around 200 °C, and the quality of graphene is further improved. This can be observed by a significant reduction in the defect in graphene after annealing (Figure S4).

2.3. Effects of Photolithography on As-Transferred and HMDS-Treated Graphene. As-transferred graphene and HMDS-treated graphene substrates were patterned using AZ5214E photoresist before the photoresist was removed with acetone. AZ5214E was chosen as it is widely employed in microfabrication and can be used as a positive and image reversal photoresist. Figure 4 shows the Raman map of as-transferred graphene, as-transferred graphene after photolithography, and graphene treated with HMDS after the lithography process. The Raman scan area is 20 μm × 20 μm. Both the first-order G peak and the second-order 2D peak are present in the Raman spectra; the D-peak is absent for as-transferred samples. This indicates that graphene has a very low defect density. The G and 2D peaks of the as-transferred samples are centered at 1587 and 2683 cm^{-1}, respectively, with an FWHM value of the G peak of 18 cm^{-1}. This indicates that as-transferred graphene exhibits hole doping, which could be due to the presence of water absorbents or substrate impurities. The hole doping is reduced after HMDS, which can be observed as downshifts of 2 and 3 cm^{-1} for the 2D and G peaks in HMDS samples. The influence of doping can be observed from the ratio between 2D/G peaks. The average I_{2D}/I_G peaks ratio for nontreated and HMDS-treated samples are 2.18 and 2.42, respectively. The increase in I_{2D}/I_G ratio after HMDS treatment indicates that doping is reduced with HMDS treatment. Photolithography does not introduce doping in graphene after HMDS, which may be because the HMDS acts as a protective layer preventing any direct contact between graphene and photoresist. Another feature that can be

https://dx.doi.org/10.1021/acsomega.0c05631
ACS Omega 2021, 6, 4767−4775

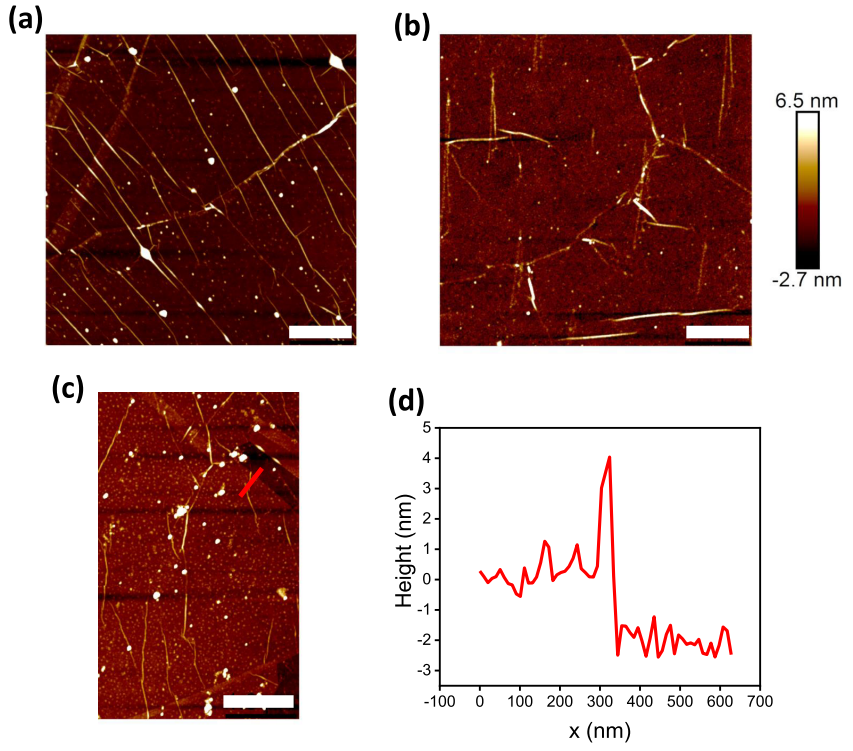

Figure 5. AFM characteristics of bare Gr and Gr modification with HMDS. (a) Bare Gr. (b) and (c) Gr after HMDS treatment. (d) Line profile shows the height of the HMDS layer on Gr. Scale bars = 1 μm.

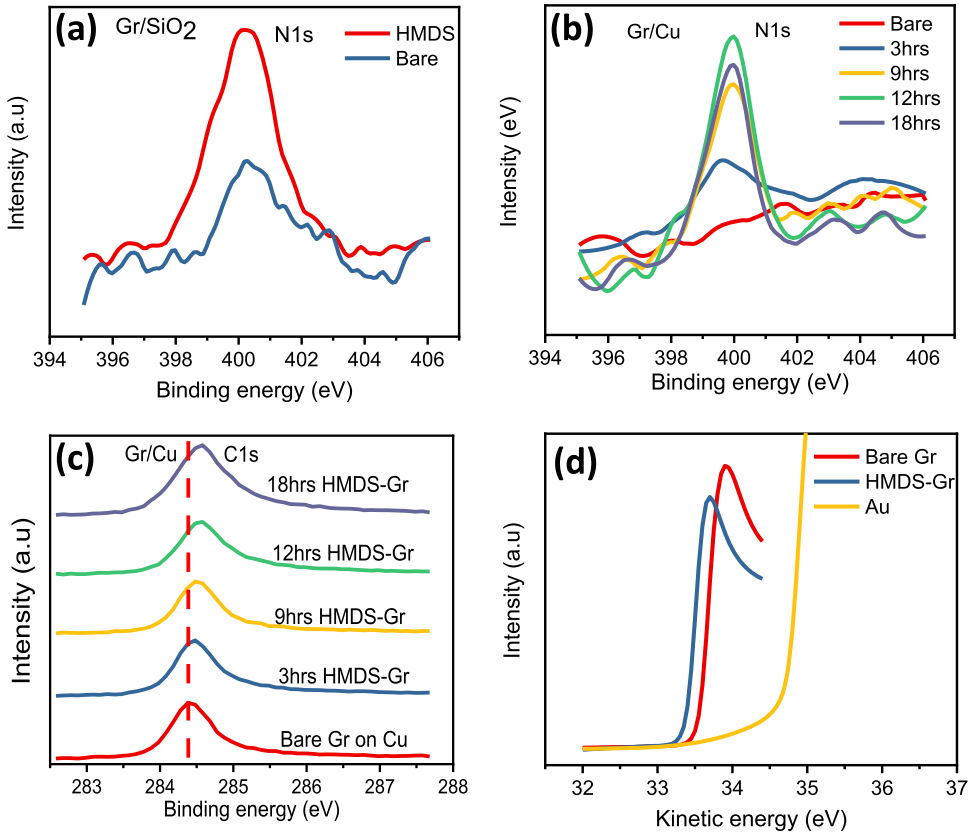

Figure 6. (a) N 1s XPS spectrum of as-transferred and HMDS-treated graphene on the SiO_2/Si substrate. (b) N 1s XPS spectrum of as-grown and HMDS-treated graphene on Cu. (c) Evolution of the C 1s peak as a function of the HMDS treatment of Gr on Cu. (d) XPS spectra of Gr, Gr-HMDS, and Au at the secondary electron energy region with substrate bias at −30 V.

https://dx.doi.org/10.1021/acsomega.0c05631
ACS Omega 2021, 6, 4767−4775

observed from the Raman spectrum is the presence of the D-peak at ∼1340 cm^{-1}, illustrating defects introduced into graphene during the photolithography process. An increase in I_D/I_G peak intensity of as-transferred graphene after photoresist was observed without HMDS treatment, the HMDS-treated graphene shows a negligible D-peak, indicating that the HMDS protects the graphene layer and prevents direct contact between graphene and photoresist. HMDS is compatible with photoresist, and therefore leaving the sample in HMDS with photoresist does not degrade or damage the photoresist.

2.4. Effect of HMDS Treatment Time on the Surface of Graphene. The presence of HMDS on the graphene surface was first characterized using atomic force microscopy (AFM). The surface roughness of graphene increased from 0.3 nm without HMDS to 0.5 nm after HMDS treatment (Figure 5a,b). The thickness of HMDS on the graphene surface was approximately determined using line profile to be around 1.3−1.8 nm, as shown in Figure 5c,d. We further performed X-ray photoelectron spectroscopy (XPS) and water contact angle (WCA) measurements to characterize the surface of graphene after HMDS treatment to investigate the effect of HMDS treatment on the electronic properties of graphene and to determine the optimum treatment time. XPS was used first to analyze surface properties and the presence of HMDS on the surface of Gr/SiO_2/Si substrates. The N 1s peak at a binding energy of ∼400 eV is significantly enhanced after the HMDS treatment of graphene compared to as-transferred samples (Figure 6a). The presence of nitrogen in the as-transferred samples could be introduced during the graphene transfer process. This could be due to the reaction of ammonium persulfate (APS) or RCA1 cleaning in the form of ammonium hydroxide with defects and edges in graphene.[51,52] XPS spectra of the two samples are shown in Figures S5 and S6. To reduce the effects of the substrate and the transfer process, we have performed the XPS analysis by coating HMDS on Gr/Cu and by conducting a comparison with as-grown graphene on copper.

The N 1s spectrum of as-grown Gr on Cu shows no presence of nitrogen species on graphene, as shown in Figure 6b. On the other hand, HMDS-treated graphene samples show an N 1s peak at ∼399.9 eV. The longer the samples were immersed in HMDS, the stronger the N 1s signal is with no obvious improvement after 12 h treatment (Further XPS analysis is shown in Figures S7 and S8). Furthermore, we compared the peak position of C 1s in bare Gr/Cu with HMDS-Gr/Cu with different HMDS treatment durations. It is interesting to note that the position of the peak is blue-shifted toward higher binding energy with increasing exposure to HMDS, as shown in Figure 6c. The maximum shift observed is ∼0.15 eV after 12 h HMDS treatment (The deconvolution of C 1s peak and the position of the C−C sp^2 peak position as a function of HMDS treatment time are shown in Figure S9), which suggests a change in Fermi level in graphene as a reduction of p-doping due to removal of water after HMDS treatment.[29,44,53]

We measured the change in the work function of as-transferred graphene with that of HMDS-treated graphene to determine the effect of HMDS treatment on its electronic properties. The change in work function is measured using XPS with Al irradiation source of the photon energy of $h\nu$ = 1486.6 eV. The sample was biased with a negative potential of −30 V applied to the substrate. The work function is then calculated using the following equation:

$$\varnothing = h\nu - |E_{\text{Cut-off}} - E_F| \quad (5)$$

where $E_{\text{Cut-off}}$ is the secondary electron energy cutoff. Figure 6d shows the XPS spectra for as-transferred graphene, HMDS-treated graphene, and Au. The work function of graphene is reduced by ∼0.20 eV after coating with HMDS. This reduction in work function of graphene after HMDS treatment is in close agreement with the value of Fermi energy shift of 0.14 eV as observed in the transfer characteristics of the GFETs after HMDS treatment extracted from eq 1. The small difference between the two values could be attributed to the effect of contacts to graphene that cause doping in graphene underneath the contact region. The origin of this decrease in work function could be partly attributed to the removal of water and oxygen absorbents from its surface after HMDS treatment. The untreated graphene exhibits p-doping characteristics due to water molecules at its surface due to its electron-withdrawing character. The dipole moment in water can induce a shift in Fermi level in graphene.[54] We calculated the change in work function due to the contribution of water dipole moment by[44,55]

$$\Delta\Phi = \frac{\Gamma \mu_z \cos\theta}{\varepsilon\varepsilon_0} \quad (6)$$

where $\Gamma \approx 5 \times 10^{13}$ cm^{-2} is the density of water molecules accumulate on the graphene surface; ε_0 is the permittivity of the free space; $\varepsilon \approx 2$ is the relative dielectric constant of a few layers of water;[56] μ_z = 1.85 D is the dipole moment of water molecule normal to the surface;[57] and θ is the angle of the dipole from the surface normal. The approximate change in work function induced by water dipole moment is estimated to be 0.12 eV.

The dipole moment in HMDS is also expected to affect the graphene electronic properties by screening the impurities directly underneath graphene. However, such role is less significant because HMDS has weaker dipole moment compared with water.[58] Furthermore, our results show that HMDS reduces the traps/defects induced during the processing of graphene. Our results are also supported by the observation of negligible hysteresis in graphene transistors after HMDS treatment as an indication of the role of HMDS in removing water molecules and screening out the charge impurities in graphene[58,59] (Figure S10). It was noticeable that the interaction between graphene and water changes after the application of HMDS due to the hydrophobic properties of HMDS layer, and the surface of the graphene becomes more hydrophobic with HMDS modifications. Figure S11 shows the evolution of the water contact angle (WCA) of graphene on the SiO_2/Si substrate after different durations of HMDS treatment. The WCA was recorded over 10 s with 330 frames and a droplet size of ∼30 μL. The WCA of graphene changes by about 12° after 12 h treatment with HMDS.

In this study, a solution-processed HMDS was used to modify graphene with SAMs. However, for long-term stability and shorter processing time, vapor-processed HMDS could be more beneficial.

3. CONCLUSIONS

In summary, we have demonstrated that the passivation of the graphene surface with the self-assembled monolayers of HMDS has significantly improved the quality of graphene after thin-film deposition and device manufacturing. Through the application of HMDS to the graphene surface prior to

https://dx.doi.org/10.1021/acsomega.0c05631
ACS Omega 2021, 6, 4767−4775

lithography and contact deposition, a direct contact between the graphene and photoresist is prevented. The HMDS functions as a protective layer for the graphene during plasma processing. As a result, the concentration of the D-peak is reduced more than 2-fold after HMDS treatment and the contact resistance of graphene has been improved more than doubled compared with that of as-transferred graphene. Therefore, the HMDS protection of graphene is expected to enable the deposition of gate dielectric and metal electrodes on graphene with preserving the high quality of graphene. This approach is compatible with microfabrication processing and offers a simple solution for the fabrication of high-quality graphene-field-effect devices.

4. EXPERIMENTAL SECTION

Graphene preparation: Monolayer graphene grown by CVD on Cu foil was coated with 300 nm poly(methyl methcrylate) (PMMA) to support the graphene transfer. The PMMA was cured in ambient conditions for 12 h. Graphene at the backside of Cu foil was etched using oxygen plasma for 1 min at power 75 W. The Cu was then etched using ammonium persulfate (APS) (0.01 g/mL in H_2O) overnight. The PMMA/graphene stack is then floated on two consecutive ultra DI water baths to rinse the graphene surface for up to 1 h per bath. The PMMA/graphene was then transferred onto modified RCA1 solution (20:1:1 $H_2O/H_2O_2/NH_4OH$) for 1 h at room temperature to remove Cu residues followed by two steps of ultra DI water bath for 1 h each. The freestanding PMMA/graphene layer was transferred to a SiO_2/Si substrate. The PMMA/graphene on the substrate was baked on a hotplate for 2 h at 150 °C to improve the adhesion of graphene to the substrate. PMMA was then removed using acetone for 5 h followed by isopropanol (IPA) for 5 min. The sample was then annealed at 200 °C for 6 h to remove PMMA residues on the graphene surface.

Raman spectroscopy measurements were performed using a confocal Witec spectrometer and exited with a laser wavelength of 532 nm (excitation energy $E_L = \hbar w_L = 2.33\ eV$) through an optical fiber, and an objective lens of 100X, NA = 0.8, and laser spot of 0.4 μm. The laser power was kept below 2 mW and a spectral resolution was ~3 cm^{-1}; the Raman peak position was calibrated based on the Si peak position at 520.7 cm^{-1}. The D, G, and 2D peaks were fitted with Lorenzian functions.

X-ray photoelectron spectroscopy (XPS) experiments and measurements were performed with Kα^+ and an Al radiation source ($h\nu$ = 1486.6 eV) in an ultrahigh vacuum chamber for spectroscopic analysis with a base pressure of 5×10^{-8} mbar.

Fabrication and electrical measurements of graphene contact structures: For metal contact structures, graphene on Si/SiO_2 substrates was patterned using optical lithography, then sets of samples were immersed in HMDS for 12 h in the exposed contact region and the other set kept in a desiccator. Typically, 5/50 nm Ti/Au was deposited on the sample. Finally, the lift-off process was performed using acetone to remove the photoresist. Two-probe measurements were used to measure the contact characteristics of the CTLM structures. The measurements were performed at room temperature using B1500 Semiconductor Analyzer.

For GFETs, graphene on Si/SiO_2 substrates was patterned using optical lithography and oxygen plasma to define the device structure. Another lithography step followed by the sputtering process and lift-off were used to form 5/50 nm Ti/Au. Three-probe measurements were used to measure the transfer characteristics of GFETs with back-gate.

Contact angle measurements: a Theta optical tensiometer was used to measure the static contact angle. A droplet of water 30 μL in size was deposited onto the surface of the graphene and the measurements were taken within a 10 s frame. The contact angle was then determined by fitting the Young−Laplace equation around the droplet. Graphene samples clean and free of defects were selected for contact angle measurements to reduce the error that could be caused by a defective surface.

DC and rf sputtering experiments: two sets of $Gr/Si/SiO_2$ substrates were prepared. One was immersed in fresh HMDS solution overnight and the other was kept in ambient conditions. The substrates were placed in a sputter chamber at ultrahigh vacuum conditions of 1×10^{-7} mbar. The sputtering process was performed at pressure levels between 6.0 and 8.5×10^{-3} mbar in the presence of Ar. In the case of DC sputtering, the power was set to 60 W and the deposition rate was 0.2 Å/s, while power levels of 90 and 100 W were used for rf sputtering with deposition rates of 0.07 and 0.08 Å/s.

Photoresist experiments: two sets of $Gr/Si/SiO_2$ substrates were prepared. One was immersed in fresh HMDS solution for 6 h and the other was kept in ambient conditions. AZ5214E was spun-coated on the substrates, and the samples were soft baked on a hotplate at 90 °C for 3 min. Both sets of samples were exposed to UV light with an intensity of around 80 mJ/cm^2 before they developed using an MF319 developer.

■ ASSOCIATED CONTENT

Supporting Information

The Supporting Information is available free of charge at https://pubs.acs.org/doi/10.1021/acsomega.0c05631.

Two-probe measurements with and without HMDS, Raman measurements of graphene with and without HMDS after rf Al sputtering with 100 W compared with as-transferred graphene, and XPS spectra of graphene with and without HMDS on SiO_2 and Cu (PDF)

■ AUTHOR INFORMATION

Corresponding Author

Sami Ramadan − *Department of Materials, Imperial College London, London SW7 2AZ, U.K.*; orcid.org/0000-0002-0013-731X; Email: s.ramadan@imperial.ac.uk

Authors

Yuanzhou Zhang − *Department of Materials, Imperial College London, London SW7 2AZ, U.K.*

Deana Kwong Hong Tsang − *Department of Materials, Imperial College London, London SW7 2AZ, U.K.*

Olena Shaforost − *Department of Materials, Imperial College London, London SW7 2AZ, U.K.*

Lizhou Xu − *Department of Materials, Imperial College London, London SW7 2AZ, U.K.*

Ryan Bower − *Department of Materials, Imperial College London, London SW7 2AZ, U.K.*; orcid.org/0000-0002-3519-0532

Iain E. Dunlop − *Department of Materials, Imperial College London, London SW7 2AZ, U.K.*; orcid.org/0000-0002-6329-4996

https://dx.doi.org/10.1021/acsomega.0c05631
ACS Omega 2021, 6, 4767−4775

Peter K. Petrov − *Department of Materials, Imperial College London, London SW7 2AZ, U.K.;* orcid.org/0000-0003-3643-6685

Norbert Klein − *Department of Materials, Imperial College London, London SW7 2AZ, U.K.*

Complete contact information is available at: https://pubs.acs.org/10.1021/acsomega.0c05631

Notes

The authors declare no competing financial interest.

■ ACKNOWLEDGMENTS

This research is funded by the UK's Engineering and Physical Sciences Research Council (EPSRC) under contract No. EP/P02985X/1. The authors would like to thank Dr. Wenqian Chen for his useful discussions and suggestions.

■ REFERENCES

(1) Geim, A. K. Graphene: Status and Prospects. *Science* **2009**, *324*, 1530−1534.
(2) Geim, A. K.; Novoselov, K. S. The rise of graphene. *Nat. Mater.* **2007**, *6*, 183.
(3) Lin, Y.-M.; Dimitrakopoulos, C.; Jenkins, K. A.; Farmer, D. B.; Chiu, H.-Y.; Grill, A.; Avouris, P. 100-GHz Transistors from Wafer-Scale Epitaxial Graphene. *Science* **2010**, *327*, 662.
(4) Wu, Y.; Lin, Y.-m.; Bol, A. A.; Jenkins, K. A.; Xia, F.; Farmer, D. B.; Zhu, Y.; Avouris, P. High-frequency, Scaled Graphene Transistors on Diamond-like carbon. *Nature* **2011**, *472*, 74.
(5) Yan, H.; Li, X.; Chandra, B.; Tulevski, G.; Wu, Y.; Freitag, M.; Zhu, W.; Avouris, P.; Xia, F. Tunable infrared plasmonic devices using graphene/insulator stacks. *Nat. Nanotechnol.* **2012**, *7*, 330.
(6) Ju, L.; Geng, B.; Horng, J.; Girit, C.; Martin, M.; Hao, Z.; Bechtel, H. A.; Liang, X.; Zettl, A.; Shen, Y. R.; Wang, F. Graphene plasmonics for tunable terahertz metamaterials. *Nat. Nanotechnol.* **2011**, *6*, 630.
(7) Adabi, M.; Lischner, J.; Hanham, S. M.; Mihai, A. P.; Shaforost, O.; Wang, R.; Hao, L.; Petrov, P. K.; Klein, N. Microwave Study of Field-Effect Devices Based on Graphene/Aluminum Nitride/Graphene Structures. *Sci. Rep.* **2017**, *7*, No. 44202.
(8) Will, M.; Hamer, M.; Müller, M.; Noury, A.; Weber, P.; Bachtold, A.; Gorbachev, R. V.; Stampfer, C.; Güttinger, J. High Quality Factor Graphene-Based Two-Dimensional Heterostructure Mechanical Resonator. *Nano Lett.* **2017**, *17*, 5950−5955.
(9) Eichler, A.; Moser, J.; Chaste, J.; Zdrojek, M.; Wilson-Rae, I.; Bachtold, A. Nonlinear Damping in Mechanical Resonators Made from Carbon Nanotubes and Graphene. *Nat. Nanotechnol.* **2011**, *6*, 339.
(10) Mahmoudi, T.; Wang, Y.; Hahn, Y.-B. Graphene and its Derivatives for Solar Cells Application. *Nano Energy* **2018**, *47*, 51−65.
(11) Hu, H.; Yang, X.; Guo, X.; Khaliji, K.; Biswas, S. R.; García de Abajo, F. J.; Low, T.; Sun, Z.; Dai, Q. Gas identification with graphene plasmons. *Nat. Commun.* **2019**, *10*, No. 1131.
(12) Schedin, F.; Geim, A. K.; Morozov, S. V.; Hill, E. W.; Blake, P.; Katsnelson, M. I.; Novoselov, K. S. Detection of individual gas molecules adsorbed on graphene. *Nat. Mater.* **2007**, *6*, 652.
(13) Yuan, W.; Shi, G. Graphene-based gas sensors. *J. Mater. Chem. A* **2013**, *1*, 10078−10091.
(14) Park, S. J.; Kwon, O. S.; Lee, S. H.; Song, H. S.; Park, T. H.; Jang, J. Ultrasensitive Flexible Graphene Based Field-Effect Transistor (FET)-Type Bioelectronic Nose. *Nano Lett.* **2012**, *12*, 5082−5090.
(15) Zheng, C.; Huang, L.; Zhang, H.; Sun, Z.; Zhang, Z.; Zhang, G.-J. Fabrication of Ultrasensitive Field-Effect Transistor DNA Biosensors by a Directional Transfer Technique Based on CVD-Grown Graphene. *ACS Appl. Mater. Interfaces* **2015**, *7*, 16953−16959.
(16) Xu, L.; Li, D.; Ramadan, S.; Li, Y.; Klein, N. Facile biosensors for rapid detection of COVID-19. *Biosens. Bioelectron.* **2020**, *170*, No. 112673.
(17) Tang, X.; Reckinger, N.; Poncelet, O.; Louette, P.; Ureña, F.; Idrissi, H.; Turner, S.; Cabosart, D.; Colomer, J.-F.; Raskin, J.-P.; Hackens, B.; Francis, L. A. Damage evaluation in graphene underlying atomic layer deposition dielectrics. *Sci. Rep.* **2015**, *5*, No. 13523.
(18) Li, Z.; Chen, F. Ion beam modification of two-dimensional materials: Characterization, properties, and applications. *Appl. Phys. Rev.* **2017**, *4*, No. 011103.
(19) Ahlberg, P.; Johansson, F. O. L.; Zhang, Z.-B.; Jansson, U.; Zhang, S.-L.; Lindblad, A.; Nyberg, T. Defect formation in graphene during low-energy ion bombardment. *APL Mater.* **2016**, *4*, No. 046104.
(20) Vervuurt, R. H. J.; Kessels, W. M. M.; Bol, A. A. Atomic Layer Deposition for Graphene Device Integration. *Adv. Mater. Interfaces* **2017**, *4*, No. 1700232.
(21) Liu, W. J.; Yu, H. Y.; Wei, J.; Li, M. F. Impact of Process Induced Defects on the Contact Characteristics of Ti/Graphene Devices. *Electrochem. Solid-State Lett.* **2011**, *14*, K67−K69.
(22) Kang, S.; Movva, H. C. P.; Sanne, A.; Rai, A.; Banerjee, S. K. Influence of electron-beam lithography exposure current level on the transport characteristics of graphene field effect transistors. *J. Appl. Phys.* **2016**, *119*, No. 124502.
(23) Fan, J.; Michalik, J. M.; Casado, L.; Roddaro, S.; Ibarra, M. R.; De Teresa, J. M. Investigation of the influence on graphene by using electron-beam and photo-lithography. *Solid State Commun.* **2011**, *151*, 1574−1578.
(24) Jang, C. W.; Kim, J. H.; Kim, J. M.; Shin, D. H.; Kim, S.; Choi, S. H. Rapid-thermal-annealing surface treatment for restoring the intrinsic properties of graphene field-effect transistors. *Nanotechnology* **2013**, *24*, No. 405301.
(25) Sagade, A. A.; Neumaier, D.; Schall, D.; Otto, M.; Pesquera, A.; Centeno, A.; Elorza, A. Z.; Kurz, H. Highly air stable passivation of graphene based field effect devices. *Nanoscale* **2015**, *7*, 3558−3564.
(26) Kim, S.; Nah, J.; Jo, I.; Shahrjerdi, D.; Colombo, L.; Yao, Z.; Tutuc, E.; Banerjee, S. K. Realization of a high mobility dual-gated graphene field-effect transistor with Al_2O_3 dielectric. *Appl. Phys. Lett.* **2009**, *94*, No. 062107.
(27) Ahlberg, P.; Hinnemo, M.; Song, M.; Gao, X.; Olsson, J.; Zhang, S.-L.; Zhang, Z.-B. A two-in-one process for reliable graphene transistors processed with photo-lithography. *Appl. Phys. Lett.* **2015**, *107*, No. 203104.
(28) Lee, W. H.; Park, Y. D. Tuning Electrical Properties of 2D Materials by Self-Assembled Monolayers. *Adv. Mater. Interfaces* **2018**, *5*, No. 1700316.
(29) Park, J.; Lee, W. H.; Huh, S.; Sim, S. H.; Kim, S. B.; Cho, K.; Hong, B. H.; Kim, K. S. Work-Function Engineering of Graphene Electrodes by Self-Assembled Monolayers for High-Performance Organic Field-Effect Transistors. *J. Phys. Chem. Lett.* **2011**, *2*, 841−845.
(30) Lafkioti, M.; Krauss, B.; Lohmann, T.; Zschieschang, U.; Klauk, H.; Klitzing, Kv.; Smet, J. H. Graphene on a Hydrophobic Substrate: Doping Reduction and Hysteresis Suppression under Ambient Conditions. *Nano Lett.* **2010**, *10*, 1149−1153.
(31) Lee, W. H.; Park, J.; Kim, Y.; Kim, K. S.; Hong, B. H.; Cho, K. Control of Graphene Field-Effect Transistors by Interfacial Hydrophobic Self-Assembled Monolayers. *Adv. Mater.* **2011**, *23*, 3460−3464.
(32) Kitzmann, J.; Göritz, A.; Fraschke, M.; Lukosius, M.; Wenger, C.; Wolff, A.; Lupina, G. Perfluorodecyltrichlorosilane-based seed-layer for improved chemical vapour deposition of ultrathin hafnium dioxide films on graphene. *Sci. Rep.* **2016**, *6*, No. 29223.
(33) Jeon, J. H.; Jerng, S.-K.; Akbar, K.; Chun, S.-H. Hydrophobic Surface Treatment and Interrupted Atomic Layer Deposition for Highly Resistive Al_2O_3 Films on Graphene. *ACS Appl. Mater. Interfaces* **2016**, *8*, 29637−29641.
(34) Tu, Q.; Kim, H. S.; Oweida, T. J.; Parlak, Z.; Yingling, Y. G.; Zauscher, S. Interfacial Mechanical Properties of Graphene on Self-Assembled Monolayers: Experiments and Simulations. *ACS Appl. Mater. Interfaces* **2017**, *9*, 10203−10213.

(35) Chowdhury, S. F.; Sonde, S.; Rahimi, S.; Tao, L.; Banerjee, S.; Akinwande, D. Improvement of graphene field-effect transistors by hexamethyldisilazane surface treatment. *Appl. Phys. Lett.* **2014**, *105*, No. 033117.
(36) Thodkar, K.; Thompson, D.; Lüönd, F.; Moser, L.; Overney, F.; Marot, L.; Schönenberger, C.; Jeanneret, B.; Calame, M. Restoring the Electrical Properties of CVD Graphene via Physisorption of Molecular Adsorbates. *ACS Appl. Mater. Interfaces* **2017**, *9*, 25014−25022.
(37) Politou, M.; Asselberghs, I.; Radu, I.; Conard, T.; Richard, O.; Lee, C. S.; Martens, K.; Sayan, S.; Huyghebaert, C.; Tokei, Z.; Gendt, S. D.; Heyns, M. Transition metal contacts to graphene. *Appl. Phys. Lett.* **2015**, *107*, No. 153104.
(38) Schroder, D. K. *Semiconductor Material and Device Characterization*; Wiley-Interscience, 2006.
(39) Nagashio, K.; Toriumi, A. Density-of-States Limited Contact Resistance in Graphene Field-Effect Transistors. *Jpn. J. Appl. Phys.* **2011**, *50*, No. 070108.
(40) Liu, W.; Wei, J.; Sun, X.; Yu, H. A Study on Graphene—Metal Contact. *Crystals* **2013**, *3*, 257−274.
(41) Li, B.; Pan, G.; Jamil, N. Y.; Al Taan, L.; Awan, S.; Avent, N. Shielding technique for deposition of Au electrical contacts on graphene by sputtering. *J. Vac. Sci. Technol., A* **2015**, *33*, No. 030601.
(42) Nagashio, K.; Nishimura, T.; Kita, K.; Toriumi, A. In *Metal/Graphene Contact as A Performance Killer of Ultra-high Mobility Graphene Analysis of Intrinsic Mobility and Contact Resistance*, IEEE International Electron Devices Meeting (IEDM) 7−9 Dec, 2009; pp 1−4.
(43) Giubileo, F.; Di Bartolomeo, A. The role of contact resistance in graphene field-effect devices. *Prog. Surf. Sci.* **2017**, *92*, 143−175.
(44) Cernetic, N.; Wu, S.; Davies, J. A.; Krueger, B. W.; Hutchins, D. O.; Xu, X.; Ma, H.; Jen, A. K. Y. Systematic Doping Control of CVD Graphene Transistors with Functionalized Aromatic Self-Assembled Monolayers. *Adv. Funct. Mater.* **2014**, *24*, 3464−3470.
(45) Pisana, S.; Lazzeri, M.; Casiraghi, C.; Novoselov, K. S.; Geim, A. K.; Ferrari, A. C.; Mauri, F. Breakdown of the adiabatic Born−Oppenheimer approximation in graphene. *Nat. Mater.* **2007**, *6*, 198−201.
(46) Lee, J. E.; Ahn, G.; Shim, J.; Lee, Y. S.; Ryu, S. Optical separation of mechanical strain from charge doping in graphene. *Nat. Commun.* **2012**, *3*, No. 1024.
(47) Cançado, L. G.; Jorio, A.; Ferreira, E. H. M.; Stavale, F.; Achete, C. A.; Capaz, R. B.; Moutinho, M. V. O.; Lombardo, A.; Kulmala, T. S.; Ferrari, A. C. Quantifying Defects in Graphene via Raman Spectroscopy at Different Excitation Energies. *Nano Lett.* **2011**, *11*, 3190−3196.
(48) Froehlicher, G.; Berciaud, S. Raman spectroscopy of electrochemically gated graphene transistors: Geometrical capacitance, electron-phonon, electron-electron, and electron-defect scattering. *Phys. Rev. B* **2015**, *91*, No. 205413.
(49) Srivastava, P. K.; Ghosh, S. Defect engineering as a versatile route to estimate various scattering mechanisms in monolayer graphene on solid substrates. *Nanoscale* **2015**, *7*, 16079−16086.
(50) Wang, Z.; Yao, Q.; Eigler, S. Room-Temperature Transport Properties of Graphene with Defects Derived from Oxo-Graphene. *Chem. - Eur. J.* **2020**, *26*, 6484−6489.
(51) Wang, X.; Li, X.; Zhang, L.; Yoon, Y.; Weber, P. K.; Wang, H.; Guo, J.; Dai, H. N-Doping of Graphene Through Electrothermal Reactions with Ammonia. *Science* **2009**, *324*, 768−771.
(52) Wang, G.; Jia, L.-T.; Zhu, Y.; Hou, B.; Li, D.-B.; Sun, Y.-H. Novel preparation of nitrogen-doped graphene in various forms with aqueous ammonia under mild conditions. *RSC Adv.* **2012**, *2*, 11249−11252.
(53) Geng, H.-Z.; Kim, K. K.; So, K. P.; Lee, Y. S.; Chang, Y.; Lee, Y. H. Effect of Acid Treatment on Carbon Nanotube-Based Flexible Transparent Conducting Films. *J. Am. Chem. Soc.* **2007**, *129*, 7758−7759.
(54) Moser, J.; Verdaguer, A.; Jiménez, D.; Barreiro, A.; Bachtold, A. The environment of graphene probed by electrostatic force microscopy. *Appl. Phys. Lett.* **2008**, *92*, No. 123507.
(55) Koh, S. E.; McDonald, K. D.; Holt, D. H.; Dulcey, C. S.; Chaney, J. A.; Pehrsson, P. E. Phenylphosphonic Acid Functionalization of Indium Tin Oxide: Surface Chemistry and Work Functions. *Langmuir* **2006**, *22*, 6249−6255.
(56) Fumagalli, L.; Esfandiar, A.; Fabregas, R.; Hu, S.; Ares, P.; Janardanan, A.; Yang, Q.; Radha, B.; Taniguchi, T.; Watanabe, K.; Gomila, G.; Novoselov, K. S.; Geim, A. K. Anomalously low dielectric constant of confined water. *Science* **2018**, *360*, 1339.
(57) Leenaerts, O.; Partoens, B.; Peeters, F. M. Water on graphene: Hydrophobicity and dipole moment using density functional theory. *Phys. Rev. B* **2009**, *79*, No. 235440.
(58) Ku, G. M.; Lee, E.; Kang, B.; Lee, J. H.; Cho, K.; Lee, W. H. Relationship between the dipole moment of self-assembled monolayers incorporated in graphene transistors and device electrical stabilities. *RSC Adv.* **2017**, *7*, 27100−27104.
(59) Xu, H.; Chen, Y.; Zhang, J.; Zhang, H. Investigating the Mechanism of Hysteresis Effect in Graphene Electrical Field Device Fabricated on SiO2 Substrates using Raman Spectroscopy. *Small* **2012**, *8*, 2833−2840.

https://dx.doi.org/10.1021/acsomega.0c05631
ACS Omega 2021, 6, 4767−4775